INTERPOLATION BETWEEN IMAGES BY CONSTRAINED OPTIMAL TRANSPORT

Said Kerrache and Yasushi Nakauchi
Graduate School of Systems and Information Engineering, University of Tsukuba, 1-1-1 Tennodai, Tsukuba, Japan

Keywords: Constrained optimal transport, Monge-Kantorovich, Interpolation between images.

Abstract: In this paper, the recently proposed technique of constrained optimal transport is used to interpolate between images under specified constraints. The intensity values in both images are considered as mass distributions, and a flow of minimum kinetic energy is computed to transport the initial distribution to the final one, while satisfying specified constraints on the intermediate mass as well as the the velocity or the momentum field. As an application, the proposed method is used for interpolating between images with a common unchanged part, as well as under constraint on the volume expansion and contraction. The latter is achieved by imposing bounds on the divergence of the velocity field of the flow. This constraint is discretized then integrated into the problem Lagrangian using the augmented Lagrangian method. A variation of the solution is also presented, where the constraint is decoupled into two constraints coordinated by an additional Lagrange multiplier. This allows a considerable speedup, though numerical robustness decreases in certain cases. Constrained optimal transport can potentially be used in image registration. In particular, the proposed method for controlling the volume change has potential application in registration of images under volume change constraints as it is the case for medical images depicting muscle movements or those with contrast enhancing structures.

1 INTRODUCTION

Interpolation between images is a basic task used in many areas of computer graphics and computer vision (Beier and Neely, 1992; Schaefer et al., 2006; Stich et al., 2008; Manning and Dyer, 1999; Seitz and Dyer, 1996) . Given two images, the goal of image interpolation is to find a continuous sequence of images that transforms one image to the other. There is a large number of interpolation techniques, the most simple of which is linear interpolation. In practice, however, more sophisticated techniques are used, notably the thin-plate spline interpolation method (see (Wolberg, 1998) for a survey). Image interpolation is tightly linked to image registration. Indeed, many techniques for image registration achieve the desired transformation by gradually deforming one image to the other (Zitova, 2003). Like image registration, the interpolation problem is ill-posed, and consequently, there may be a large (even infinite theoretically) number of interpolations that can match two images. However, it is important to consider only those interpolations that cause a reasonable deformation to the image. For instance, transformations that cause extreme distortions of the image, folding for instance, are excluded. This can be achieved using a number of techniques, of which the method of optimal transport is of particular interest to this work . In this method, the images are considered as mass distributions, and a map that minimizes the transport cost between the two images is sought (Haker et al., 2004).

Optimal transport is a field that is attracting an increasing number of researchers and is increasingly applied in various fields in mathematics, science and technology (Villani, 2009). Within the field of image registration, optimal transport belongs to the fluid registration category (Bro-Nielsen and Gramkow, 1996), and it is in many respects related to the optical flow technique (Beauchemin and Barron, 1995). It has been applied successfully for registering various types of images (Haker et al., 2004; Museyko et al., 2009). Despite this, optimal transport suffers from a number of shortcomings. First, it offers no control on the intermediate images, which may sometimes lead to undesired interpolations . Indeed, depending on the field of application, often there may be some physical (or medical) considerations that limit the type of applicable transformations (Haber and Modersitzki, 2004b; Rohlfing et al., 2003). For instance, interpolations that lead to objects colliding or occupying the same space may be rejected (see Figure 5 and Section 4 for an example). This is an example where intermediate

Kerrache S. and Nakauchi Y..
INTERPOLATION BETWEEN IMAGES BY CONSTRAINED OPTIMAL TRANSPORT.
DOI: 10.5220/0003375200750084
In *Proceedings of the International Conference on Computer Vision Theory and Applications* (VISAPP-2011), pages 75-84
ISBN: 978-989-8425-47-8

images are constrained. As another example, muscles such as the heart can shrink and expand, but within a certain limit (Haber et al., 2010). In this case, it is the relative change in volume that must be constrained. Furthermore, and as it is the case with many fluid registration techniques, optimal transport can result in extreme deformations leading to topological changes or unreasonable expansions or contractions of the different image regions. Figure 1 shows the interpolation between two synthetic images that differ by a simple translation using optimal transport. Figure 2, on the other hand, shows the interpolation between the same two images using a divergence free flow. The two results seem only slightly different. However, a closer look at the divergence of the optimal transport flow in Figure 3 shows that the image is not translated as in the case of the divergence-free flow, but instead, the region of high intensity is expanded, whereas the region of low intensity is shrunk. This is the result of minimizing the kinetic energy: only the difference in mass is transported, not the whole mass in the region. Here again, limiting the relative change in volume would avoid such unreasonable transformations.

In this paper, we use the method of constrained optimal transport (Kerrache and Nakauchi, 2011) to interpolate between images. Constraints on the interpolation: intermediate images as well as relative change in volume can be imposed. Mathematically, the relative change in volume is simply the Jacobian of the transformation. Imposing a bound on the Jacobian can be achieved by bounding the divergence of the velocity field as it shown in Section 3. Aside from the interpolation itself, an additional motivation for this work is constrained image registration. Indeed, once the interpolation is computed it becomes possible to compute the map between the two images by integrating the velocity field of the flow. This point will be the subject of a further study. The remainder of this paper is organized as follows. Section 2 presents the notion of constrained optimal transport. Section 3 presents the proposed method. Section 4 contains the experimental results of the proposed algorithms. Finally, Section 5 concludes the paper and gives some future research directions.

2 CONSTRAINED OPTIMAL TRANSPORT

Optimal transport admits two distinct formulations. In the time-independent formulation, the problem data consist in two spaces, each supporting a probability measure. The goal is to find a mass- preserving map between the two spaces that minimizes a certain transport cost. The cost can be the distance traveled by each particle of mass, a function of the distance or otherwise. In the time-dependent formulation, the supporting space is the same, and the task consists in transporting an initial mass distribution to a final configuration. The cost in the time-dependent case is also related to the distance between source and destination, but it has a continuous description. Each curve joining any two points is given a cost, and therefore, the transport cost is dependent on the path followed and not only the start and ending points. Under appropriate assumptions (Villani, 2009), the transport between two mass distributions can be interpreted as traversing a path in the set of probability measures over the space under consideration. Finding an optimal transport consists then in finding a minimizing curve in the space of probabilities. This formulation is used by (Kerrache and Nakauchi, 2011) to introduce the concept of constrained optimal transport, where certain curves in the space of probability measures are declared infeasible and can not be used as transport paths. This allows to formulate a number of interesting problems. For instance, it is possible to eliminate certain mass distributions, or eliminate transport plans that cause certain changes to the initial density. This is the case in this paper, where transport plans that cause undesired intermediate images or deformations are eliminated.

In (Benamou and Brenier, 2000), the problem of optimal mass transport in a closed convex subset D of $\mathcal{R}^d$ with the squared Euclidean distance as cost is transformed to an optimal control problem of a potential flow (Cohen and Kundu, 2004). The approach consists in computing a flow, in the sens of fluid dynamics, having the minimum kinetic energy that moves the initial density to the final one. More precisely, the problem is formulated as

$$\inf_{\rho,m} \int_0^1 \int_D \frac{|m(t,x)|^2}{2\rho(t,x)} dxdt, \tag{1}$$

$$\text{s.t. } \partial_t \rho + \nabla \cdot m = 0, \tag{2}$$

$$\rho(0,\cdot) = \rho_0, \quad \rho(1,\cdot) = \rho_1, \tag{3}$$

where $\rho(t,x)$ is the density, $m(t,x)$ is the momentum of the flow, $\rho_0(x)$ and $\rho_1(x)$ are two bounded positive density functions defined on D, such as

$$\int_D \rho_0(x)\,dx = \int_D \rho_1(x)\,dx = 1$$

This problem is then transformed to the following saddle point problem

$$\inf_{\phi,q} \sup_{\mu} \mathcal{L}(\phi,q,\mu) = F(q) + G(\phi) + \langle \mu, \nabla\phi - q \rangle, \tag{4}$$

where $\mu = (\rho, m)$, $G(\phi) = \int_D \phi(0,x)\rho_0(x) - \phi(1,x)\rho_1(x)\,dx$, F is defined by

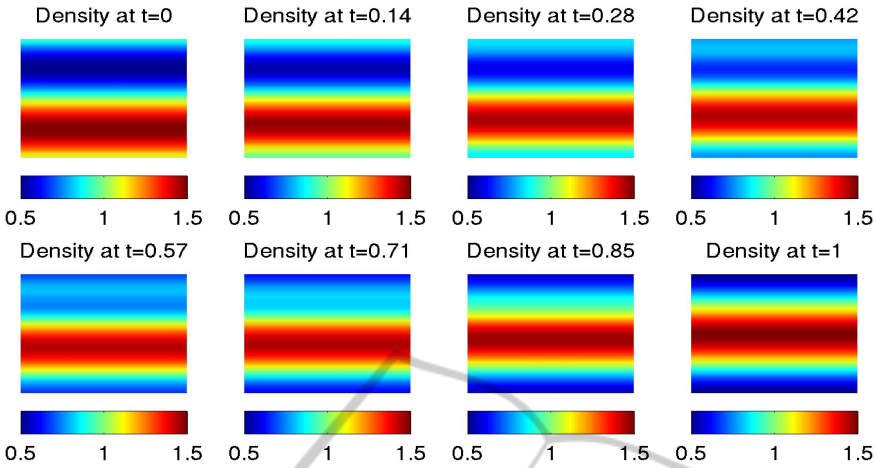

Figure 1: Interpolation using optimal transport.

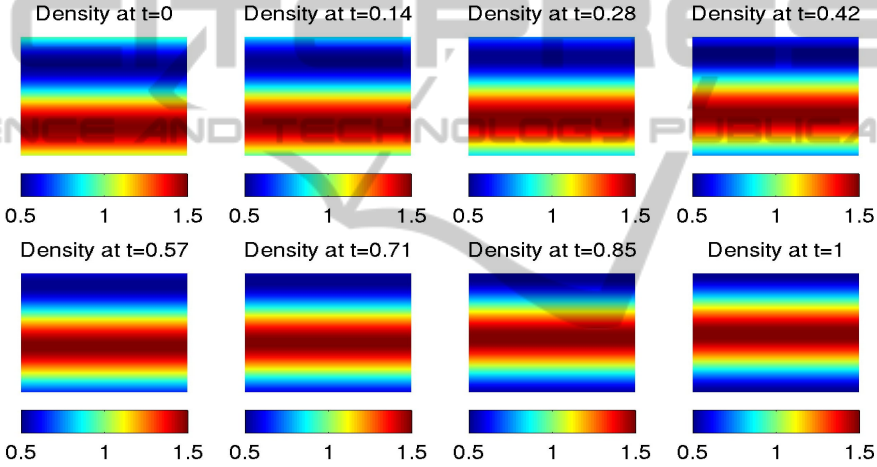

Figure 2: Interpolation using a divergence-free flow.

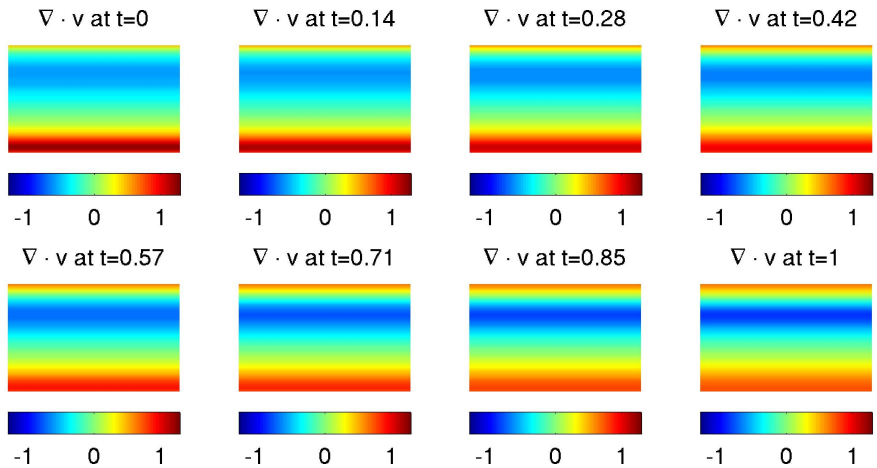

Figure 3: The divergence of the optimal transport flow.

$$F(q) = \begin{cases} 0 & \text{if } q \in K, \\ +\infty & \text{otherwise,} \end{cases}$$

with

$$K = \left\{ (a,b) : \mathcal{R} \times \mathcal{R}^d \to \mathcal{R} \times \mathcal{R}^d, \; a + \frac{|b|^2}{2} \leq 0 \text{ pointwise} \right\},$$

and $\langle \cdot, \cdot \rangle$ is the inner product defined by

$$\langle u, v \rangle = \int_0^1 \int_D u \cdot v. \tag{5}$$

This formulation allowed the authors to devise an algorithm to compute the optimal flow by an Uzawa type algorithm, the description of which can be found in (Fortin and Glowinski, 1983) and (Glowinski and Tallec, 1989). The maximization over μ, which is a free variable in Problem (4), implies that $|\nabla\phi - q|$ must be zero at the saddle point. This allowed the authors to augment Lagrangian by the term $r/2\,|\nabla\phi - q|^2$, where r is a positive constant. Problem (4) is thus transformed to

$$\inf_{\phi,q} \sup_{\mu} \mathcal{L}(\phi, q, \mu) = F(q) + G(\phi) + \langle \mu, \nabla\phi - q \rangle + \frac{r}{2} |\nabla\phi - q|^2. \tag{6}$$

The authors then present a numerical scheme for solving Problem (6), where ϕ, q and μ are updated iteratively. The computation of ϕ consists in solving a Poisson equation, q is obtained by solving a pointwise optimization problem, whereas μ is updated using a gradient-type rule.

In (Kerrache and Nakauchi, 2011), Problem (1) is solved under the additional constraint that $\mu = (\rho, m) \in U$, where U is a closed convex set. With this additional constraint, $|\nabla\phi - q|$ is not guaranteed to reach 0. In fact, $|\nabla\phi - q|$ not reaching zero indicates that the constraint is active. Because of this, it is not possible to use the same approach as previously, and the problem is rewritten by introducing new decoupling variables and Lagrange multipliers. Furthermore, the Lagrangian is augmented with additional quadratic terms that improve the quality of the numerical algorithms. The new form is (see (Kerrache and Nakauchi, 2011)):

$$\inf_{\phi,q,p,b} \sup_{\mu \in U, \nu, \eta} \mathcal{L}_{r,s}(\phi, q, p, b, \mu, \nu, \eta) = F(q) + G(\phi) + \langle \mu, p - b \rangle + \langle \nu, \nabla\phi - p \rangle + \langle \eta, b - q \rangle + \frac{r}{2} |\nabla\phi - p|^2 + \frac{r}{2} |b - q|^2 - \frac{s}{2} |\mu - \nu|^2 - \frac{s}{2} |\mu - \eta|^2. \tag{7}$$

Here r and s are positive numbers, p and b are decoupling variables and ν, η are the new Lagrange multipliers. The authors then present a number of Uzawa type algorithms to solve Problem (7).

3 THE PROPOSED METHOD

The interpolation between two images is achieved by computing a flow of minimum kinetic energy that transports the intensity values of the first image to match those in the second one. This of course assumes that both images have the same total amount of intensity values, which can be achieved by normalizing both images (Haker et al., 2004). Using constrained optimal transport, it is possible to impose constraints on the intermediate interpolation. For instance, it is possible to fix a part of the image that is common to both the initial and the final images during the interpolation process. An example exploiting this idea is presented in the section of experiment results. Similarly, it is possible to isolate different parts of the image and interpolate them independently by forcing the normal components of the momentum to be null at the boundaries of each portion.

A more complex type of constraints can be imposed on the divergence of the velocity field, which translates into a constraint on the rate of expansion and contraction of the image content. Indeed, the transformation created by the fluid flow can be computed by integrating in time the path that each particle follows. A particle initially at (x_0, y_0) follows a path that verifies the following system of ordinary differential equations:

$$\begin{cases} dx/dt = v_x(x(t), y(t), t) \\ dy/dt = v_y(x(t), y(t), t) \end{cases}$$

with initial conditions (x_0, y_0). Here v_x and v_y are the components of the velocity field of the flow. The map that associates to each point (x, y) the point $(x(t), y(t))$ solution to the above system of equations is called the flow map and denoted by $\varphi(x,t)$ or $\varphi_t(x)$. The transformation caused by the flow is therefore φ_1, that is the map that associates to each point its final destination. A classical result in fluid dynamics is that the Jacobian $J(x,t)$ of φ_t evolves under the relation (see (Chorin and Marsden, 1993)):

$$\frac{\partial}{\partial t} J(x,t) = \nabla \cdot v(\varphi(x,t),t)\, J(x,t),$$

where v is the velocity field of the flow. If we impose the condition

$$\alpha \leq \nabla \cdot v(x,t) \leq \beta, \quad \forall x \in D, \tag{8}$$

and assume that $J(x,t)$ is strictly positive, then it follows that

$$\alpha \leq \int_0^1 \frac{\frac{\partial}{\partial t} J(x,t)}{J(x,t)} dt \leq \beta.$$

Since at $t = 0$, φ is the identity map, we have that $\exp(\alpha) \leq J(x,1) \leq \exp(\beta)$. Therefore, controlling the divergence of the velocity field allows the control of the Jacobian of the transformation. The advantage of this approach is that instead of a strong non-linear constraint on the determinant of the flow map, we have a much simpler one, which is linear in the velocity field. Notice that the constraint is enforced pointwise, which is much stronger than a constraint on the average.

An important observation is that the mass preservation condition and the constraint on the volume expansion and contraction can be contradictory. Indeed, preserving and matching the mass, which in the case of images represents the intensity, may require a minimum change in the volume. Therefore, the bounds on the Jacobian must be reasonably chosen. Furthermore, the constraint (8) is non-convex as a function of μ, which implies that local optimization algorithms as those presented in this paper may find a local minimum only, depending on the initial values of the variables.

3.1 Optimization

There are two approaches that can be used to solve a constrained transport problem. The first is to project the variable μ onto the feasible set at each iteration. This method is used in Algorithm 1 presented hereafter, which is proposed in (Kerrache and Nakauchi, 2011). In this algorithm and the following ones, V, H, H', H'' are Hilbert spaces of functions and vector fields over the computational domain equipped with inner products analogous to (5) and the associated norms. For fixed μ, p and b, the two Lagrangians $\mathcal{L}_{p,\mu}$ and $\mathcal{L}_{b,\mu}$ appearing in the algorithms are defined by

$$\mathcal{L}_{p,\mu}(\phi,\nu) = G(\phi) + \langle \nu, \nabla\phi - p \rangle + \frac{r}{2}|\nabla\phi - p|^2 - \frac{s}{2}|\nu - \mu|^2,$$

$$\mathcal{L}_{b,\mu}(q,\eta) = F(q) + \langle \eta, b - q \rangle + \frac{r}{2}|q - b|^2 - \frac{s}{2}|\eta - \mu|^2.$$

These Lagrangians are introduced merely for simplifying notation.

Algorithm 1 (Kerrache and Nakauchi, 2011)

- Initialization: $\left(p^0, b^0, \mu^0, \nu^0, \eta^0\right) \in H \times H \times U \times H \times H$ given arbitrarily.
- Repeat the following steps until convergence.
  1. Compute ϕ^n such that: $\mathcal{L}_{p^{n-1},\mu^n}\left(\phi^n, \nu^{n-1}\right) \leq \mathcal{L}_{p^{n-1},\mu^n}\left(\phi, \nu^{n-1}\right), \quad \forall \phi \in V;$
  2. $p^n = p^{n-1} - \rho_r\left(\mu^n - \nu^{n-1} + r\left(p^{n-1} - \nabla\phi^n\right)\right);$
  3. $\nu^n = \nu^{n-1} + \rho_s\left(\nabla\phi^n - p^{n-1} - s\left(\nu^{n-1} - \mu^n\right)\right);$
  4. Compute q^n such that: $\mathcal{L}_{b^{n-1},\mu^n}\left(q^n, \eta^{n-1}\right) \leq \mathcal{L}_{b^{n-1},\mu^n}\left(q, \eta^{n-1}\right), \quad \forall (q,\eta) \in H \times H;$
  5. $b^n = b^{n-1} - \rho_r\left(\eta^{n-1} - \mu^n + r\left(b^{n-1} - q^n\right)\right);$
  6. $\eta^n = \eta^{n-1} + \rho_s\left(b^{n-1} - q^n - s\left(\eta^{n-1} - \mu^n\right)\right);$
  7. $\mu^{n+1} = \arg\inf_{\mu \in U} |\mu - \frac{1}{2}\left(\nu^n + \eta^n + \frac{1}{s}\left(p^n - b^n\right)\right)|^2.$

As shown in (Kerrache and Nakauchi, 2011), computing ϕ^n is equivalent to solving the Poisson equation $-r\Delta\phi = \nabla \cdot \left(\nu^{n-1} - rp^{n-1}\right)$, with Neumann boundary conditions in the time dimension given by $r\partial_t\phi(0,\cdot) = \rho_0 - \nu_0^n(0,\cdot) + rp_0^{n-1}(0,\cdot)$ and $r\partial_t\phi(1,\cdot) = \rho_1 - \nu_0^n(1,\cdot) + rp_0^{n-1}(1,\cdot)$, where ν_0 and p_0 are the first elements of the vectors ν and p respectively. Similarly, finding q^n amounts to solving

$$\inf_{q \in K} \left| b^{n-1} + \frac{\eta^{n-1}}{r} - q \right|^2.$$

The projection method is efficient for problems with simple constraints. However, for more complex constraints that can be written as a set of a reasonable number of inequalities, a faster method is to use the augmented Lagrangian technique to enforce the constraints gradually. The cost of each iteration is significantly less than that in the projection method, since only a non-constrained, or bound-constrained, quadratic minimization is needed instead of a constrained one. The use of augmented Lagrangian has also the advantage of not requiring a feasible starting point, as it is the case for interior point methods. This is an important advantage, since finding a feasible point can be very difficult in some problems, for instance the present image interpolation task. This method is presented in Algorithm 2. Here, the Lagrangian is augmented with

$$-\frac{w}{2}|C(\mu)|^2,$$

where w is a positive number. For the problem of constrained divergence, $C(\mu)$ is taken to be $\nabla \cdot v - \omega$ for some specified constant value ω. Notice that the algorithm solves the problem with an equality constraint $C(\mu) = 0$. Inequality constraints can be handled easily by adding slack variables, in which case, Step 8 corresponds to a bound-constraint minimization.

Algorithm 2

- Initialization: $\left(p^0, b^0, \mu^0, \nu^0, \eta^0, \lambda^0\right) \in H \times H \times H \times H \times H \times H'$ given arbitrarily.
- Repeat the following steps until convergence.
  1. Compute ϕ^n such that $\mathcal{L}_{p^{n-1},\mu^n}\left(\phi^n, \nu^{n-1}\right) \leq \mathcal{L}_{p^{n-1},\mu^n}\left(\phi, \nu^{n-1}\right), \quad \forall \phi \in V$;
  2. $p^n = p^{n-1} - \rho_r\left(\mu^n - \nu^{n-1} + r\left(p^{n-1} - \nabla\phi^n\right)\right)$;
  3. $\nu^n = \nu^{n-1} + \rho_s\left(\nabla\phi^n - p^{n-1} - s\left(\nu^{n-1} - \mu^n\right)\right)$;
  4. Compute q^n such that: $\mathcal{L}_{b^{n-1},\mu^n}\left(q^n, \eta^{n-1}\right) \leq \mathcal{L}_{b^{n-1},\mu^n}\left(q, \eta^{n-1}\right), \quad \forall (q,\eta) \in H \times H$;
  5. $b^n = b^{n-1} - \rho_r\left(\eta^{n-1} - \mu^n + r\left(b^{n-1} - q^n\right)\right)$;
  6. $\eta^n = \eta^{n-1} + \rho_s\left(b^{n-1} - q^n - s\left(\eta^{n-1} - \mu^n\right)\right)$;
  7. $\mu^{n+1} = \arg\sup_{\mu \in H}\left[\langle \mu, p^n - b^n\rangle - \frac{s}{2}\left|\mu - \nu^n\right|^2 - \frac{s}{2}\left|\mu - \eta^n\right|^2 + \langle \lambda^n, C(\mu)\rangle - \frac{w}{2}\left|C(\mu)\right|^2\right]$;
  8. $\lambda^{n+1} = \lambda^n - \rho_w C\left(\mu^{n+1}\right)$.

In the algorithm, λ denotes the Lagrange multiplier for the new constraint $C(\mu) = 0$. The numbers ρ_r, ρ_s and ρ_w are stepping parameters that are chosen by the user. The choice of these parameters is important. If they are chosen too large, the algorithm diverges, whereas if chosen to small, the algorithm takes unnecessarily long time to converge.

To apply this algorithm, the divergence operator is first discretized (in the current implementation, using finite difference), then the minimization is performed on the resulting discretization. The constraint on the divergence is applied to the velocity field, which is related to μ by a nonlinear transformation:

$$v = \frac{m}{\rho}.$$

As a result, the problem of minimizing μ in Step 8 of Algorithm 2 can become time consuming when solving large problems. Indeed, the Hessian is not constant and the number of its non-zero elements grows quadratically with the size of discretization of the divergence operator. A solution to this problem is to use the Lagrange multiplier technique to decouple the relation linking the velocity and μ from the bound constraints. Accordingly, a new variable γ is added, which represents the velocity field, and a new constraint is added to the problem: $m = \rho\gamma$ (remember that $\mu = (\rho, m)$). This constraint is enforced using a Lagrange multiplier ζ, and the Lagrangian is augmented with the the quadratic term

$$-\frac{u}{2}\left|m - \rho\gamma\right|^2,$$

where u is a positive constant. The new problem can be solved using the following algorithm.

Algorithm 3

- Initialization: $\left(p^0, b^0, \mu^0, \nu^0, \eta^0, \lambda^0, \zeta^0, \gamma^0\right) \in H \times H \times H \times H \times H \times H' \times H'' \times H''$ given arbitrarily.
- Repeat the following steps until convergence.
  1. Compute ϕ^n such that $\mathcal{L}_{p^{n-1},\mu^n}\left(\phi^n, \nu^{n-1}\right) \leq \mathcal{L}_{p^{n-1},\mu^n}\left(\phi, \nu^{n-1}\right), \quad \forall \phi \in V$;
  2. $p^n = p^{n-1} - \rho_r\left(\mu^n - \nu^{n-1} + r\left(p^{n-1} - \nabla\phi^n\right)\right)$;
  3. $\nu^n = \nu^{n-1} + \rho_s\left(\nabla\phi^n - p^{n-1} - s\left(\nu^{n-1} - \mu^n\right)\right)$;
  4. Compute q^n such that: $\mathcal{L}_{b^{n-1},\mu^n}\left(q^n, \eta^{n-1}\right) \leq \mathcal{L}_{b^{n-1},\mu^n}\left(q, \eta^{n-1}\right), \quad \forall (q,\eta) \in H \times H$;
  5. $b^n = b^{n-1} - \rho_r\left(\eta^{n-1} - \mu^n + r\left(b^{n-1} - q^n\right)\right)$;
  6. $\eta^n = \eta^{n-1} + \rho_s\left(b^{n-1} - q^n - s\left(\eta^{n-1} - \mu^n\right)\right)$;
  7. $\mu^{n+1} = \arg\sup_{\mu \in H}\left[\langle \mu, p^n - b^n\rangle - \frac{s}{2}\left|\mu - \nu^n\right|^2 - \frac{s}{2}\left|\mu - \eta^n\right|^2 + \langle \zeta^n, m - \rho\gamma^n\rangle - \frac{u}{2}\left|m - \rho\gamma^n\right|^2\right]$;
  8. $\gamma^{n+1} = \arg\sup_{\gamma \in H'}\left[\langle \zeta^n, m^{n+1} - \rho^{n+1}\gamma\rangle - \frac{u}{2}\left|m^{n+1} - \rho^{n+1}\gamma\right|^2 + \langle \lambda^n, C(\gamma)\rangle - \frac{w}{2}\left|C(\gamma)\right|^2\right]$
  9. $\lambda^{n+1} = \lambda^n - \rho_w C\left(\gamma^{n+1}\right)$.
  10. $\zeta^{n+1} = \zeta^n - \rho_u\left(m^{n+1} - \rho^{n+1}\gamma^{n+1}\right)$.

In Algorithm 3, ρ_u denotes the stepping parameter for the new Lagrange multiplier, which once again must be chosen properly to strike a balance between the need for convergence and convergence speed. With this new form, the optimization problem for μ is decomposed into two optimization problems. However, both are much simpler than the original one. Indeed, both problems are quadratic, and in the case of μ, the optimization can be done pointwise. This has the effect of improving the execution time.

4 EXPERIMENTAL RESULTS

A first test of interpolation by constrained optimal transport is preformed using the images of Figure 4.

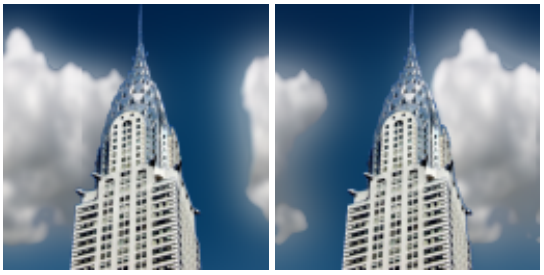

Figure 4: Test images: a building with moving clouds in the background.

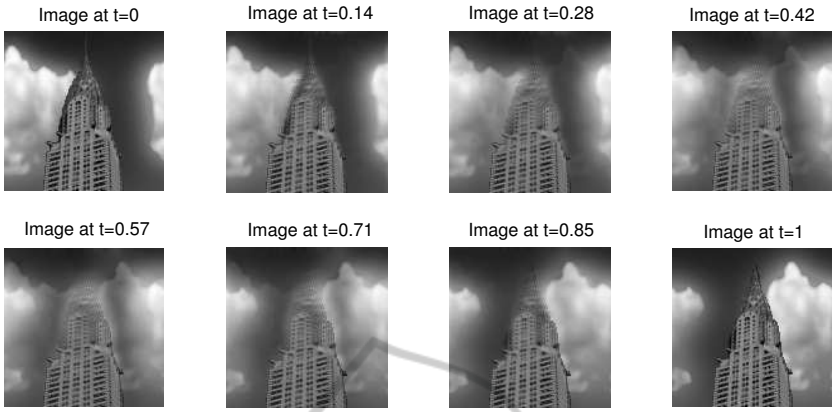

Figure 5: Interpolation using free optimal transport.

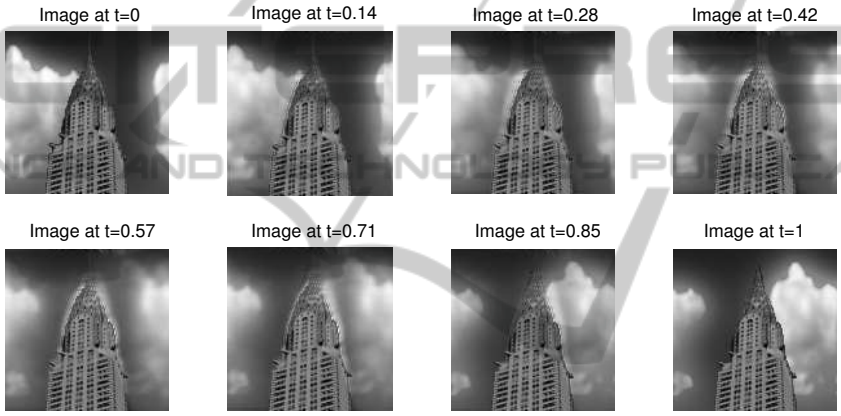

Figure 6: Interpolation using constrained optimal transport.

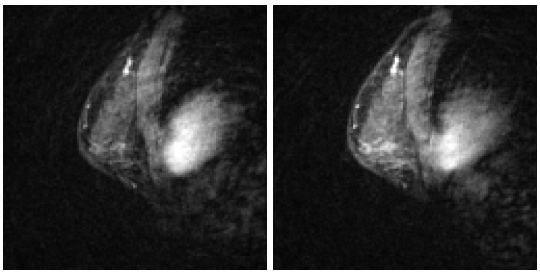

Figure 7: Test images: MRIs of a female breast, left: during the wash-in phase. right: during the wash-out phase (Haber and Modersitzki, 2004a).

In these two images, the building is a common element, whereas the background changes. Figure 5 shows the corresponding interpolation using free optimal transport. Notice that the building is distorted by the motion of the clouds. In Figure 6, a more reasonable interpolation is presented, where the building is constrained to remain constant. The solution is computed using Algorithm 1, with periodic boundary conditions.

A test of the constrained divergence interpolation method is conducted on the test images shown in Figure 7[1]. These are magnetic resonance images of a female breast. This kind of images results from injecting a marker into the body that causes an additional contrast to appear in the final image. Because

[1]Figure reproduced with permission, courtesy of IOP Publishing Ltd and the authors. Original paper available at http://dx.doi.org/10.1088/0266-5611/20/5/018

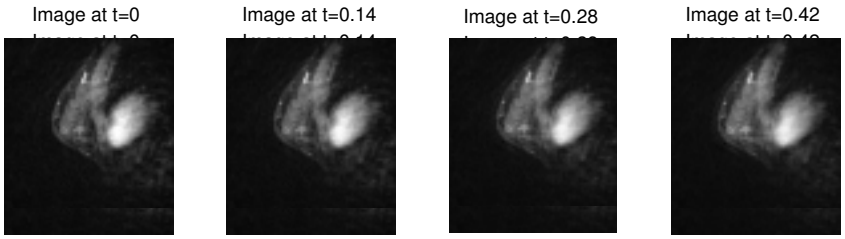

Figure 8: Interpolation using constrained optimal transport.

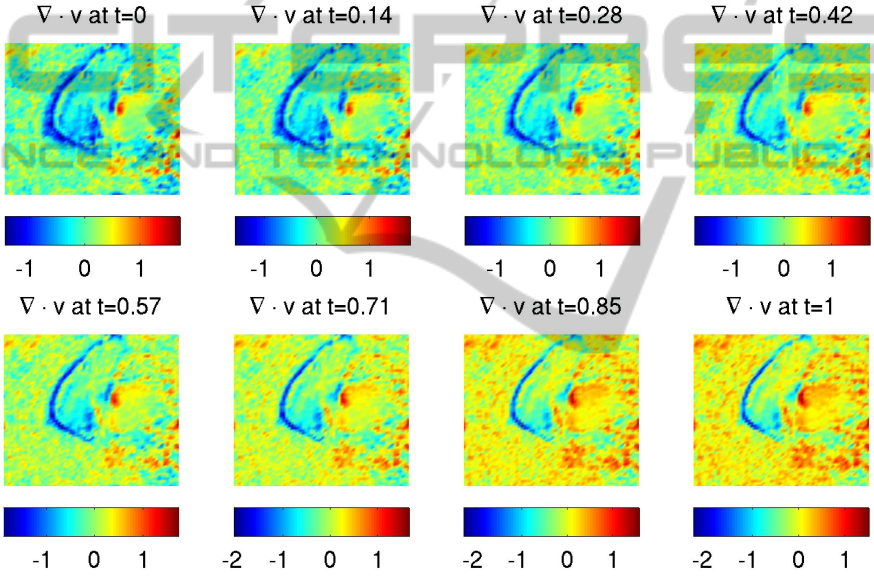

Figure 9: Divergence of the velocity field in the free case.

of this, traditional intensity based methods can not register properly these images. They cause the volume where the contrast appears to shrink considerably (see (Haber and Modersitzki, 2004a) for more details about these images and this phenomenon). The interpolation is done on these images with resolution 64 $\times$ 64. For the sake of this example, the absolute value of the divergence of the velocity field is bounded by 1.1, which limits the Jacobian, and hence the relative change of volume, between approximately 3 and 1/3 pointwise. Figure 8 shows the resulting interpolation computed by Algorithm 2. The figure shows that it is possible to achieve low volume change rates and mass preservation, while at the same time keeping the interpolation smooth. Figure 9 and 10 compare the divergence of the velocity field for the free and constrained interpolation respectively. The decrease in the divergence is clearly visible. Figure 11 and 12 show the evolution of the convergence criteria for the two algorithms. It can be seen that indeed, the energy is minimized, the constraints are being satisfied gradually and that they are active, since $|\nabla\phi - q|$ does not approach zero. To compare the two algorithms, a test is done using 32 $\times$ 32 versions of the above images. The execution time is 152 seconds for Algorithm 3 versus 257 seconds for Algorithm 3, resulting from a parallel execution on a four-core Xeon processor with enough memory. The tolerance is taken to be 5e-5. Results show that Algorithm 3 is almost twice as fast as Algorithm 2, however, it is less robust. The additional decoupling creates an oscillation phenomenon, which may cause the algorithm to miss

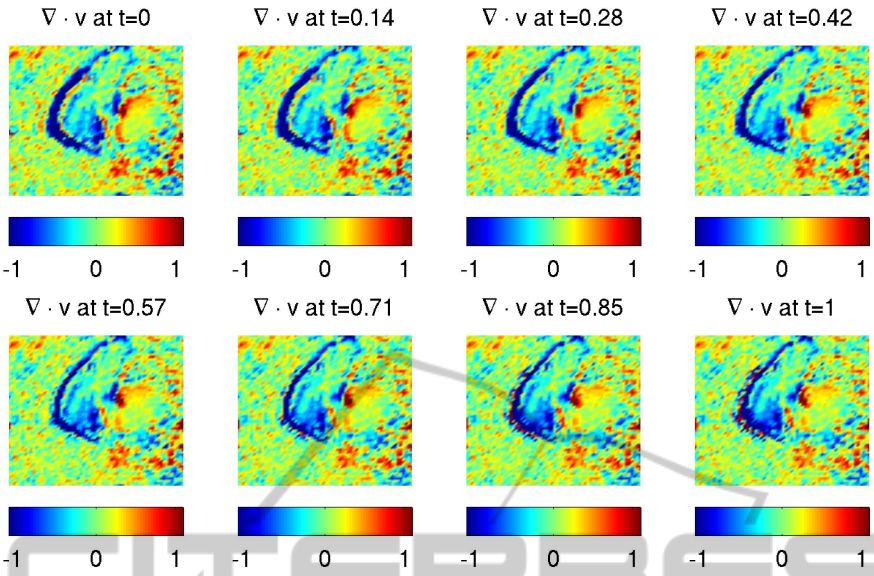

Figure 10: Divergence of the velocity field in the constrained case.

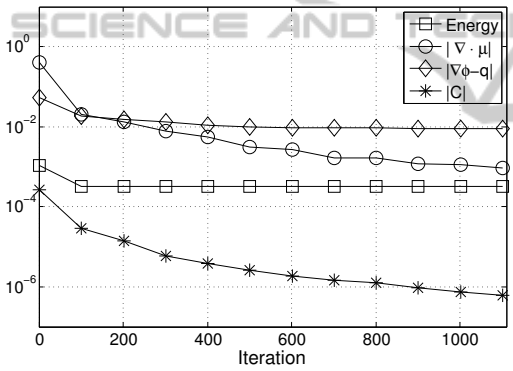

Figure 11: Trace of convergence criteria for Algorithm 2.

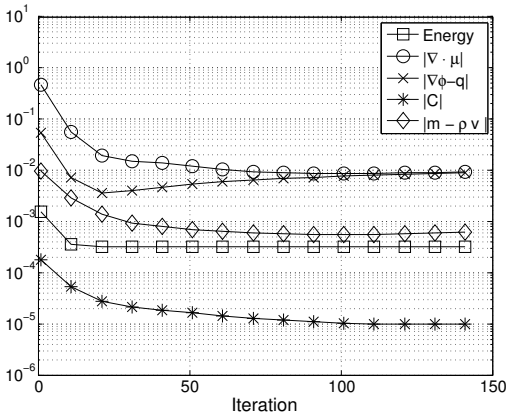

Figure 12: Trace of convergence criteria for Algorithm 3.

the saddle point and diverge when the constraint are too tight, that is small values of the bound on the divergence. Thus for problems with tight constraint, it is better to use Algorithm 2, whereas for other problems, using Algorithm 3 results in a considerable gain in time.

5 CONCLUSIONS

This paper presented a new framework for constrained image interpolation using optimal transport. Algorithms were introduced to solve the problem and numerical experiments were conducted that demonstrate their working. The proposed approach of interpolation by constrained optimal transport can be generalized to other types of constraints, as long as they can be handled by the augmented Lagrangian technique or the projection method. However, for convex constraints, such as the constraint on the divergence of the velocity field presented in this paper, the solution obtained depends heavily on the starting point. The algorithms may get stuck in a local minimum or fail to find a feasible point. This practically limits the minimum value of the absolute value of the divergence that can be achieved. As a future work, we plan on investigating methods to obtain good initial points from which to start the optimization, and techniques to escape local minima and locally infeasible regions.

Also as future direction of research, we intend to use this method for image registration, especially in medical applications. As previously explained, this requires the computation of the flow map. Although this can theoretically be easily done by integrating the velocity field, it is a challenging problem in practice, due to the compressible nature of the flows involved.

REFERENCES

Beauchemin, S. S. and Barron, J. L. (1995). The computation of optical flow. *ACM Comput. Surv.*, 27:433–466.

Beier, T. and Neely, S. (1992). Feature-based image metamorphosis. *SIGGRAPH Comput. Graph.*, 26:35–42.

Benamou, J.-D. and Brenier, Y. (2000). A computational fluid mechanics solution to the Monge-Kantorovich mass transfer problem. *Numer. Math.*, 84(3):375–393.

Bro-Nielsen, M. and Gramkow, C. (1996). Fast fluid registration of medical images. In *Proceedings of the 4th International Conference on Visualization in Biomedical Computing*, pages 267–276, London, UK. Springer-Verlag.

Chorin, A. J. and Marsden, J. E. (1993). *A Mathematical Introduction to Fluid Mechanics (Texts in Applied Mathematics) (v. 4)*. Springer.

Cohen, I. M. and Kundu, P. K. (2004). *Fluid Mechanics, Third Edition*. Academic Press.

Fortin, M. e. and Glowinski, R. e. (1983). *Augmented Lagrangian methods: Applications to the numerical solution of boundary-value problems.* Studies in Mathematics and its Applications, 15. Amsterdam-New York-Oxford: North-Holland. XIX, 340 p.

Glowinski, R. and Tallec, P. L. (1989). *Augmented Lagrangian and operator-splitting methods in nonlinear mechanics*. SIAM.

Haber, E., Horesh, R., and Modersitzki, J. (2010). Numerical optimization for constrained image registration. *Numerical Linear Algebra with Applications*, 17:343–359.

Haber, E. and Modersitzki, J. (2004a). Numerical methods for volume preserving image registration. *Inverse Problems*, 20(5):1621.

Haber, E. and Modersitzki, J. (2004b). Volume preserving image registration. In Barillot, C., Haynor, D. R., and Hellier, P., editors, *Medical Image Computing and Computer-Assisted Intervention MICCAI 2004*, volume 3216 of *Lecture Notes in Computer Science*, pages 591–598. Springer Berlin / Heidelberg.

Haker, S., Zhu, L., Tannenbaum, A., and Angenent, S. (2004). Optimal mass transport for registration and warping. *Int. J. Comput. Vision*, 60(3):225–240.

Kerrache, S. and Nakauchi, Y. (2011). Computing constrained energy-minimizing flows. In *3rd International Conference on Computer Research and Development*. Accepted.

Manning, R. A. and Dyer, C. R. (1999). Interpolating view and scene motion by dynamic view morphing. In *Proc. Computer Vision and Pattern Recognition Conf.*, volume 1, pages 388–394.

Museyko, O., Stiglmayr, M., Klamroth, K., and Leugering, G. (2009). On the application of the monge-kantorovich problem to image registration. *SIAM J. Img. Sci.*, 2(4):1068–1097.

Rohlfing, T., Maurer, C. R., Bluemke, D. A., and Jacobs, M. A. (2003). Volume-preserving nonrigid registration of MR breast images using free-form deformation with an incompressibility constraint. *Medical Imaging, IEEE Transactions on*, 22(6):730–741.

Schaefer, S., McPhail, T., and Warren, J. (2006). Image deformation using moving least squares. *ACM Trans. Graph.*, 25:533–540.

Seitz, S. M. and Dyer, C. R. (1996). View morphing. In *SIGGRAPH96*, pages 21–30.

Stich, T., Linz, C., Wallraven, C., Cunningham, D., and Magnor, M. (2008). Perception-motivated interpolation of image sequences. In *Proceedings of the 5th symposium on Applied perception in graphics and visualization*, APGV '08, pages 97–106, New York, NY, USA. ACM.

Villani, C. (2009). *Optimal transport. Old and new.* Grundlehren der Mathematischen Wissenschaften 338. Berlin: Springer. .

Wolberg, G. (1998). Image morphing: A survey. *The Visual Computer*, 14:360–372.

Zitova, B. (2003). Image registration methods: a survey. *Image and Vision Computing*, 21(11):977–1000.